THE ASTROPHYSICAL JOURNAL, 548:L33–L36, 2001 February 10

GALAXY MAPPING WITH THE SAURON INTEGRAL-FIELD SPECTROGRAPH: THE STAR FORMATION HISTORY OF NGC 4365

ROGER L. DAVIES,[1] HARALD KUNTSCHNER,[1] ERIC EMSELLEM,[2] R. BACON,[2] M. BUREAU,[3]
C. MARCELLA CAROLLO,[4] Y. COPIN,[2] BRYAN W. MILLER,[3,5] G. MONNET,[6]
REYNIER F. PELETIER,[1,7] E. K. VEROLME,[3] AND P. TIM DE ZEEUW[3]
Received 2000 September 28; accepted 2000 November 20; published 2001 February 12

ABSTRACT

We report the first wide-field mapping of the kinematics and stellar populations in the E3 galaxy NGC 4365. The velocity maps extend previous long-slit work. They show two independent kinematic subsystems: the central 300 pc × 700 pc rotates about the projected minor axis, and the main body of the galaxy, 3 kpc × 4 kpc, rotates almost at right angles to this. The line strength maps show that the metallicity of the stellar population decreases from a central value greater than solar to one-half solar at a radius of 2 kpc. The decoupled core and main body of the galaxy have the same luminosity-weighted age, ≈14 Gyr, and the same elevated magnesium-to-iron ratio. The two kinematically distinct components have thus shared a common star formation history. We infer that the galaxy underwent a sequence of mergers associated with dissipative star formation that ended ≳12 Gyr ago. The misalignment between the photometric and kinematic axes of the main body is unambiguous evidence of triaxiality. The similarity of the stellar populations in the two components suggests that the observed kinematic structure has not changed substantially in 12 Gyr.

Subject headings: galaxies: abundances — galaxies: elliptical and lenticular, cD — galaxies: evolution — galaxies: formation — galaxies: individual (NGC 4365) — galaxies: kinematics and dynamics — galaxies: stellar content

1. INTRODUCTION

The existence of decoupled cores in ≈30% of the early-type galaxies is strong evidence that mergers play an important part in the evolution of these systems (e.g., de Zeeuw & Franx 1991). Most likely, decoupled cores originate from the accretion of material with angular momentum misaligned from that of the main galaxy. A few galaxies have been studied in sufficient detail to explore when that material was accreted or whether the event was associated with gaseous dissipation and star formation. For example, in the morphologically normal galaxies IC 1459 (Franx & Illingworth 1988) and NGC 5322 (Bender 1988; Rix & White 1992) there is no difference between the colors or line strengths of the stellar populations in the decoupled core and the main galaxy. In contrast, the disturbed shell galaxy NGC 2865 shows evidence for very recent star formation in the decoupled component (Hau, Carter, & Balcells 1999).

NGC 4365 is one of the first elliptical galaxies in which minor-axis rotation was discovered (Wagner, Bender, & Möllenhoff 1988; Bender, Saglia, & Gerhard 1994). Surma & Bender (1995, hereafter SB) deduced the remarkable kinematic structure of NGC 4365 from three long-slit spectra. The main body of the galaxy rotates around its *major* axis, reaching a maximum velocity of ≈50 km s^{-1}, whereas at smaller radii ($r = 2''$–$3''$) the peak rotation velocity is 80 km s^{-1} around the *minor* axis. SB found that the decoupled core is flatter than the main galaxy (ellipticity $\epsilon_{\rm core} = 0.39$; cf. $\epsilon_{\rm main} = 0.23$). By carrying out a careful double Gaussian analysis of the kinematics, SB estimate that $V/\sigma = 1.3$ for the core, consistent with a disk or bar. They deduced that the rotating core contributes 25% of the light within $r \approx 6''$ and accounts for roughly 2% of the *total* mass. The giant elliptical galaxy in which it is embedded has a central velocity dispersion of 275 km s^{-1}. They found that the decoupled core contains a high-metallicity population with an enhanced [Mg/Fe] ratio as commonly found in giant elliptical galaxies. SB concluded that NGC 4365 is triaxial and that the formation of the core involved substantial gaseous dissipation and star formation. However, they could not distinguish formation scenarios where the merger(s) occur early ($z > 2$–3) from those where the mergers occur more recently ($z < 1$).

Hubble Space Telescope (*HST*) images reveal that NGC 4365 has a smooth intensity profile with no signs of dust, an average ellipticity of 0.26, and a very shallow central cusp. The isophotes are disky for $1'' < r < 4''$ and boxy at larger radii. At the very center ($r \lesssim 0\farcs2$) there is a blue point source (van Dokkum & Franx 1995; Carollo et al. 1997). Deep ground-based images show no evidence for shells or other morphological peculiarities out to $\approx 4r_e$ (J. P. Blakeslee 2000, private communication).

Surface brightness fluctuation measurements indicate that NGC 4365 is in the Virgo W cloud beyond the main cluster (Jensen, Tonry, & Luppino 1998). We take the distance modulus to be 31.7 mag, a distance of 22 Mpc, so that $1''$ is ≈100 pc. The effective radius r_e is $57''$, or ≈5.7 kpc (Burstein et al. 1987).

In this Letter, we present the first complete maps of the kinematics and stellar populations of NGC 4365, taken with the panoramic integral-field spectrograph SAURON (Bacon et al. 2001). In § 2, we briefly describe the observations. The kinematics and line strength index maps are presented in § 3,

[1] Department of Physics, University of Durham, South Road, Durham DH1 3LE, England, UK; roger.davies@durham.ac.uk.
[2] CRAL–Observatoire de Lyon, 9 Avenue Charles André, 69230 Saint-Genis-Laval, France.
[3] Sterrewacht Leiden, Niels Bohrweg 2, 2333 CA Leiden, Netherlands.
[4] Department of Astronomy, Columbia University, 538 West 120th Street, New York, NY 10027.
[5] Gemini Observatory, Casilla 603, La Serena, Chile.
[6] European Southern Observatory, Karl-Schwarzschild-Strasse 2, 85748 Garching, Germany.
[7] Department of Physics and Astronomy, University of Nottingham, University Park, Nottingham NG7 2RD, England, UK.

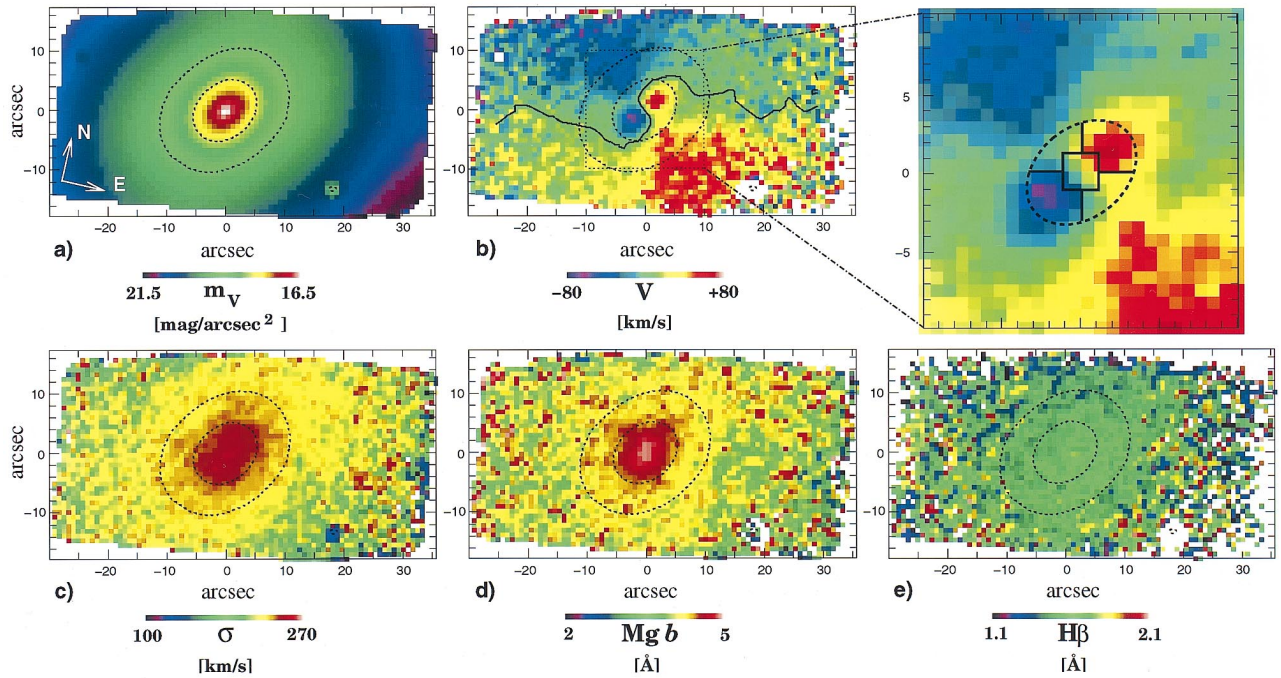

FIG. 1.—Maps of (*a*) surface brightness as reconstructed from our data, (*b*) mean streaming velocity *V*, (*c*) velocity dispersion σ, (*d*) Mg *b* line strength, and (*e*) Hβ line strength for NGC 4365. The maps are based on two partially overlapping SAURON pointings of 4 × 1800 s each, sampled with 0.″8 × 0.″8 pixels. Isophotal contours of $\mu_V = 18$ and 19 mag arcsec^{-2} are overplotted (*dotted lines*). A zero-velocity contour line (*solid black line*) is shown in (*b*). The enlarged core region of the velocity map indicates the regions that we have used for our line strength analysis. The central point is indicated by the square, the decoupled core by the sectors along the major axis, and the main body at the same radius by the sectors along the minor axis.

where we consider age-metallicity diagnostics, the Mg-σ diagram, and the spatial distribution of nonsolar abundance ratios. We discuss the implications of these results for formation scenarios in § 4 and summarize our conclusions in § 5.

2. OBSERVATIONS

We observed NGC 4365 with SAURON, mounted on the 4.2 m William Herschel Telescope on La Palma, on the nights of 2000 March 29 and 30. SAURON has a field of view of 33″ × 41″, delivering simultaneously 1431 spectra at a spectral resolution of 3.6 Å (FWHM), 0.″94 × 0.″94 spatial sampling, and 100% sky coverage (Bacon et al. 2001). Another 146 spectra are taken 1.′9 away from the main field to allow accurate sky subtraction. The wavelength range of the current setup is ≈4810–5350 Å. We observed two fields overlapping by ≈20″ on the nuclear region of NGC 4365, each field having four separate exposures of 1800 s (dithered by ≈1″, i.e., one lenslet). The combined data cubes cover a total region of 33″ × 63″ on the sky. The small offsets between the four 1800 s integrations at each position enable us to resample the final data cubes onto 0.″8 × 0.″8 pixels (drizzling technique). The effective seeing of the merged data cube was measured on three pointlike objects in the reconstructed image. It is homogeneous over the field with a value of 1.″6 ± 0.″1 (FWHM). We took arc lamp spectra before and after each individual exposure for accurate wavelength calibration.

We reduced the raw SAURON exposures by means of the algorithms described in Bacon et al. (2001). We used the individually extracted, wavelength-calibrated, and continuum-corrected spectra to derive the stellar kinematics and line strength indices as a function of (two-dimensional) position in NGC 4365. We measured the mean velocity *V* and the velocity dispersion σ with the Fourier correlation quotient method (Bender 1990) and obtained the line strength indices Hβ, Mg *b*, and Fe5270 in the Lick/IDS system (Worthey 1994), taking into account the internal velocity broadening and differences in the instrumental resolution.

3. RESULTS

Figure 1*a* shows the surface brightness distribution of NGC 4365, as reconstructed from our spectra. The reconstructed intensity map agrees well with the *HST* image after seeing convolution and binning to the SAURON spatial sampling.

Figure 1*b* shows the spectacular kinematically decoupled core of NGC 4365 in detail. The core extends ≈7″ × 3″ and rotates about the minor axis. The maximum observed core rotation speed is 80 km s^{-1} at a radius of 2.″2. The main body of the galaxy rotates slowly about an axis misaligned by 8° ± 2° with the major axis. The rotation velocity rises to 45 km s^{-1} at $r = 7''$ and remains constant at larger radii. The velocity field of the main body is not symmetric about the minor axis, and the loci of zero velocity (shown as bold line in Fig. 1*b*) and maximum velocity are not perpendicular. We will explore the consequences of this in a later paper presenting dynamical models. The velocity dispersion falls off smoothly from its central maximum of 275 km s^{-1}, and the contours of constant dispersion follow the isophotes (Fig. 1*c*). A detailed comparison shows excellent agreement with the SB long-slit data (de Zeeuw et al. 2001).

Figure 1*d* shows that the distribution of Mg *b* has a central peak, whereas the Hβ-value is roughly constant across the galaxy (Fig. 1*e*). Our average value for the central Hβ absorption strength is 1.61 ± 0.04 Å, in good agreement with the Lick/IDS measurement of 1.66 ± 0.21 Å (Trager et al. 1998). Fur-

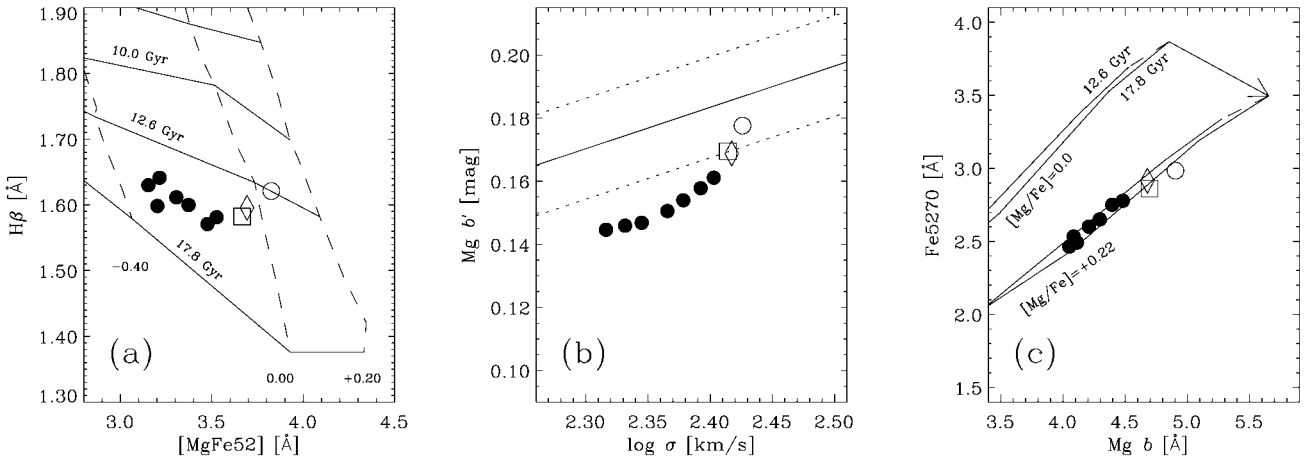

FIG. 2.—(*a*) [MgFe52] vs. Hβ equivalent width diagram. The open circle represents the average line strength of the very central data points ($r < 1\farcs6$), the open diamond represents the region of the decoupled core, and the open square reflects the mean of the data in the main body of the galaxy at the same radii as the decoupled core but along the minor axis (see also Fig. 1, enlarged core region). For larger radii, the data were averaged in elliptical annuli centered on the photometric nucleus (*filled circles*); mean semimajor-axis radii: $5\farcs6$, $7\farcs2$, $9\farcs6$, $12\farcs9$, $16\farcs0$, $19\farcs9$, and $26\farcs1$ (radius increases from right to left). Overplotted are the predictions of stellar population models from Vazdekis (1999). The solid lines are lines of constant age, and the dashed lines are lines of constant metallicity ([M/H]). (*b*) Local velocity dispersion vs. local Mg b' index. The solid line indicates the average relation for the cores of early-type galaxies (Colless et al. 1999), and the dashed lines indicate the 1 σ spread around it. (*c*) Mg *b* vs. Fe5270 equivalent width diagram. Overplotted are stellar population models from Vazdekis (1999) with solar abundance ratios for ages of 12.6 and 17.8 Gyr. In addition, a correction of the models for *nonsolar* abundance ratios of [Mg/Fe] = 0.22 dex is shown (Trager et al. 2000). The error bars on the mean line strength in a given zone are omitted for clarity as they are smaller or similar to the size of the symbols in the diagrams.

thermore, we find no indication for either [O III] λ5007 or Hβ emission in our spectra, so there is no evidence that our age estimates are affected by nebular emission.

In Figure 2*a*, we show the [MgFe52] versus Hβ age-metallicity diagnostic diagram ([MgFe52] = [Mg b × Fe5270]$^{1/2}$). In order to probe the stellar populations of the decoupled core with respect to the main galaxy, we have averaged the line strength in certain key regions (see also Fig. 1, enlarged core region). The very central region ($r < 1\farcs6$) of the galaxy is represented by an open circle. Furthermore, we have identified the decoupled core using the velocity maps, and we plot the average value for the line strengths in this region as an open diamond. Comparing this with the average line strengths of the main galaxy at the *same* radius along the minor axis (*open square*), we find that these two kinematically distinct regions have identical stellar populations. At larger radii ($r > 5\farcs0$), we averaged all lenslets in elliptical annuli (*filled circles*). The metal line strength decreases with increasing radius, and there is a small increase in Hβ absorption strength.

In order to make age and metallicity estimates, we use the Vazdekis (1999) models, which utilize the empirical stellar library of Jones (1997) to predict line strengths for a single-burst stellar population as a function of age and metallicity. The models were smoothed to the Lick/IDS resolution and include improved stellar population parameters (A. Vazdekis 2001, in preparation). The model predictions are shown in Figures 2*a* and 2*c*. The central metallicity is estimated to be 1.15 $Z_{\odot}$, decreasing toward larger radii (≈0.3 dex per dex in radius) at a roughly constant age of 14 Gyr (Fig. 2*a*). We note that the absolute age calibration of the models remains subject to systematic errors, but all our conclusions are based on relative age differences, which are much more robust. The small increase in Hβ absorption at the very center ($r \lesssim 1\farcs6$) suggests a luminosity-weighted age of ≈12 Gyr. We can account for this by superposing a younger population on that of the center: 6% of the mass in a stellar population with the same metallicity and an age of 5 Gyr is sufficient.

Figure 2*b* shows the Mg b–σ relation within NGC 4365. The central data points agree well with the relation for the cores of early-type galaxies (Colless et al. 1999), suggesting that the core properties of NGC 4365 are similar to those of other elliptical galaxies. For $r \lesssim 6''$, the local Mg b–σ relation shows a steeper slope than the global relation, but overall the gradient in this diagram is typical of similar galaxies studied by Davies, Sadler, & Peletier (1993) and Carollo & Danziger (1994).

In Figure 2*c* we plot Mg *b* versus Fe5270. Stellar population models (Vazdekis 1999) at solar abundance ratios and for ages 12.6 and 17.8 Gyr are overplotted. In these coordinates, the effects of age and metallicity are almost completely degenerate; hence, the model predictions overlap. Consistent with other giant elliptical galaxies (see, e.g., Kuntschner 1998 and Kuntschner et al. 2001), the data points for NGC 4365 lie off the solar ratio models toward larger values of Mg *b* and lower Fe5270 line strength. Using the corrections given by Trager et al. (2000), we also plot stellar population models at [Mg/Fe] = 0.22 dex, which are a good representation of the whole of NGC 4365. There is no difference between the decoupled core region and the main body of the galaxy. SB find that the magnesium-to-iron ratio is further enhanced in the very center. Our data, while marginally consistent with theirs, indicate no additional enhancement.

4. DISCUSSION

We now explore how the SAURON two-dimensional line strength maps constrain the star formation history of both the main body and the core of NGC 4365. There is a dramatic difference in the kinematics of the two regions of the galaxy, but other properties suggest that NGC 4365 is a normal elliptical galaxy and that the core and main body had a common

star formation history. Furthermore, the *K*-band surface brightness fluctuations in NGC 4365 place it among the old metal-rich elliptical galaxies (Jensen, Tonry, & Luppino 1998).

The elevated magnesium-to-iron ratio is roughly constant across the entire galaxy (a region of 4 kpc × 3 kpc). Such non-solar abundance ratios arise in populations enriched primarily with the products of Type II supernovae, either in a rapid initial burst of star formation or one skewed to massive stars (Worthey 1998). The uniformity of the elevated magnesium-to-iron ratio also suggests that the whole galaxy experienced a common star formation history, involving considerable gaseous dissipation, thus generating the high central metallicity and inward metallicity gradient. A possible formation scenario would be the merger of gas-rich fragments at high redshift. Such an event would be modest compared to the rates of star formation inferred for high-redshift submillimeter galaxies (e.g., Ivison et al. 2000). The decoupled core could originate from stars ejected into a tidal tail (with the appropriate angular momentum) as a result of a major merger that formed the bulk of the stars. These stars fall back to produce the kinematically distinct component at the center.

If star formation was taken to completion and the residual gas exhausted roughly 12 Gyr ago, then the decoupled kinematic structure in NGC 4365 must be long-lived. The misalignment of the kinematic and photometric axes show that the main body of the galaxy is triaxial, with the bulk of its stars on long-axis tubes and the stars in the core predominantly on short-axis tubes (Statler 1991; Arnold, de Zeeuw, & Hunter 1994). This is similar to the structure inferred for, e.g., NGC 4261 (Davies & Birkinshaw 1986) and NGC 4406 (Franx, Illingworth, & Heckman 1989). The full two-dimensional structure and kinematics derived from the SAURON data, when combined with our dynamical models (see, e.g., Cretton et al. 1999), will enable us to distinguish between a thin disk or a thick structure for the core.

5. CONCLUSIONS

The SAURON maps present a complete view of the kinematics and stellar populations of NGC 4365. They show two independent kinematic subsystems: the central 300 pc × 700 pc and the main body of the galaxy, rotating almost at right angles to each other. The misalignment of 82° between the photometric and kinematic axes of the main body is unambiguous evidence of triaxiality. The SAURON maps enable us to compare the stellar population in the decoupled component with that in the main body of the galaxy at the same radius. We find these populations to be indistinguishable in age, metallicity, and abundance ratios. We find an age of ≈14 Gyr and a decrease in metallicity, from larger than solar in the center to half-solar at a radius of 2 kpc ($\approx 0.4 r_e$). We suggest that NGC 4365 underwent dissipative star formation at high redshift, probably through one or more mergers. Later generations of stars formed a more centrally concentrated, metal-enriched stellar population. Star formation was complete and the residual gas was almost exhausted roughly 12 Gyr ago. This also suggests that the observed kinematics and triaxial structure are stable.

It is a pleasure to thank Rene Rutten and the ING staff, in particular, Tom Gregory, for support on La Palma. We thank Richard McDermid for assistance during the observing run. The SAURON project is made possible through grants 614.13.003 and 781.74.203 from ASTRON/NWO, PPARC grant "Extragalactic Astronomy and Cosmology at Durham 1998-2002," and financial contributions from the Institut National des Sciences de l'Univers, the Université Claude Bernard Lyon I, together with the universities of Durham and Leiden. R. L. D. gratefully acknowledges the award of a Research Fellowship from the Leverhulme Trust.

REFERENCES

Arnold, R. A., de Zeeuw, P. T., & Hunter, C. 1994, MNRAS, 271, 924
Bacon, R., et al. 2001, MNRAS, submitted
Bender, R. 1988, A&A, 202, L5
———. 1990, A&A, 229, 441
Bender, R., Saglia, R. P., & Gerhard, O. E. 1994, MNRAS, 269, 785
Burstein, D., Davies, R. L., Dressler, A., Faber, S. M., Stone, R. P. S., Lynden-Bell, D., Terlevich, R. J., & Wegner, G. 1987, ApJS, 64, 601
Carollo, C. M., & Danziger, I. J. 1994, MNRAS, 270, 523
Carollo, C. M., Franx, M., Illingworth, G. D., & Forbes, D. 1997, ApJ, 481, 710
Colless, M., Burstein, D., Davies, R. L., McMahan, R. K., Saglia, R. P., & Wegner, G. 1999, MNRAS, 303, 813
Cretton, N., de Zeeuw, P. T., van der Marel, R. P., & Rix, H.-W. 1999, ApJS, 124, 383
Davies, R. L., & Birkinshaw, M. 1986, ApJ, 303, L45
Davies, R. L., Sadler, E. M., & Peletier, R. F. 1993, MNRAS, 262, 650
de Zeeuw, P. T., & Franx, M. 1991, ARA&A, 29, 239
de Zeeuw, P. T., et al. 2001, MNRAS, submitted
Franx, M., & Illingworth, G. D. 1988, ApJ, 327, L55
Franx, M., Illingworth, G., & Heckman, T. 1989, ApJ, 344, 613
Hau, G. K. T., Carter, D., & Balcells, M. 1999, MNRAS, 306, 437
Ivison, R. J., Smail, I., Barger, A. J., Kneib, J., Blain, A. W., Owen, F. N., Kerr, T. H., & Cowie, L. L. 2000, MNRAS, 315, 209
Jensen, J. B., Tonry, J. L., & Luppino, G. A. 1998, ApJ, 505, 111
Jones, L. A. 1997, Ph.D. thesis, Univ. North Carolina, Chapel Hill
Kuntschner, H. 1998, Ph.D. thesis, Univ. Durham
Kuntschner, H., Lucey, J. R., Smith, S. J., Hudson, M. J., & Davies, R. L. 2001, MNRAS, in press
Rix, H.-W., & White, S. D. M. 1992, MNRAS, 254, 389
Statler, T. S. 1991, ApJ, 382, L11
Surma, P., & Bender, R. 1995, A&A, 298, 405 (SB)
Trager, S. C., Faber, S. M., Worthey, G., & González, J. J. 2000, AJ, 119, 1645
Trager, S. C., Worthey, G., Faber, S. M., Burstein, D., & González, J. J. 1998, ApJS, 116, 1
van Dokkum, P. G., & Franx, M. 1995, AJ, 110, 2027
Vazdekis, A. 1999, ApJ, 513, 224
Wagner, S. J., Bender, R., & Möllenhoff, C. 1988, A&A, 195, L5
Worthey, G. 1994, ApJS, 95, 107
———. 1998, PASP, 110, 888